



**Effect of Co or Ni substitution on magnetism in the layered van der Waals ferromagnet  $\text{Fe}_3\text{GaTe}_2$** Kejia Zhu <sup>1</sup>, Mingjie Wang,<sup>1</sup> Yazhou Deng,<sup>1</sup> Mingliang Tian,<sup>1</sup> Bin Lei,<sup>1,\*</sup> and Xianhui Chen <sup>2,3,4,†</sup><sup>1</sup>*School of Physics and Optoelectronic Engineering, Anhui University, Hefei, Anhui 230601, China*<sup>2</sup>*Department of Physics and CAS Key Laboratory of Strongly-coupled Quantum Matter Physics, University of Science and Technology of China, Hefei, Anhui 230026, China*<sup>3</sup>*CAS Center for Excellence in Quantum Information and Quantum Physics, Hefei, Anhui 230026, China*<sup>4</sup>*Collaborative Innovation Center of Advanced Microstructures, Nanjing University, Nanjing, Jiangsu 210093, China*

(Received 29 June 2023; accepted 16 February 2024; published 4 March 2024)

We have grown a series of single crystals of two-dimensional van der Waals ferromagnet  $\text{Fe}_3\text{GaTe}_2$  substituted with Co or Ni. The large single crystals of  $(\text{Fe}_{1-x}\text{Co}_x)_3\text{GaTe}_2$  ( $0 \leq x \leq 0.55$ ) and  $(\text{Fe}_{1-x}\text{Ni}_x)_3\text{GaTe}_2$  ( $0 \leq x \leq 0.46$ ) were characterized with x-ray diffraction, magnetic susceptibility, electrical resistivity, and Hall measurements. Our results show that the magnetic transition temperatures of  $\text{Fe}_3\text{GaTe}_2$  are gradually suppressed upon Co or Ni doping. A small amount of Co or Ni doping results in a significant increase of the coercive field. In particular, Co doping tunes the crystals from ferromagnetism to antiferromagnetism and then to the spin-glass state, while Ni doping tunes the crystals from ferromagnetism to spin-glass states. The strong doping-dependent magnetic properties suggest that  $\text{Fe}_3\text{GaTe}_2$  has great potential for spintronic applications.

DOI: [10.1103/PhysRevB.109.104402](https://doi.org/10.1103/PhysRevB.109.104402)**I. INTRODUCTION**

In the past decades, research on two-dimensional (2D) materials has attracted great attention due to their interesting physical properties and potential applications [1–11]. In particular, the recent discovery of 2D magnetic materials, which presents intrinsic ferromagnetic/antiferromagnetic (FM/AFM) ground states at finite temperatures down to atomic-layer thicknesses, offers possibilities for both fundamental research and the potential applications of spintronic devices [9–11]. Layer-dependent magnetism in a van der Waals (vdW) crystal down to the monolayer limit has been reported in few-layered  $\text{CrI}_3$  [9].  $\text{Cr}_2\text{Ge}_2\text{Te}_6$  has displayed a highly sensitive and thickness-dependent ferromagnetic transition to external magnetic fields [10]. Monolayer  $\text{Fe}_3\text{GeTe}_2$  has also been shown to host intrinsic 2D ferromagnetism with a Curie temperature ( $T_C$ ) of 20 K [11]. These 2D magnetic materials are mainly mechanically exfoliated from their layered bulk materials. The layered vdW ferromagnets facilitate their atomic-layer cleavability and magnetic anisotropy, which counteract spin fluctuations, thereby providing an ideal platform for theoretically and experimentally exploring quantum phenomena in the 2D limit. Despite extensive research on vdW materials, it is striking that very few studies have focused on layered vdW magnetic materials.

Among these layered vdW magnetic materials, the  $\text{Fe}_N\text{GeTe}_2$  ( $N = 3, 4, 5$ ) family is particularly remarkable due to its high Curie temperature and vast tunability of magnetic properties [11–20]. Chemical substitution, as a conventional approach to manipulate the physical properties of magnetic

materials, has been widely reported in  $\text{Fe}_N\text{GeTe}_2$  system [21–29]. For instance, a record high  $T_C = 478$  K has been achieved by Ni substitution in  $\text{Fe}_5\text{GeTe}_2$  [22], the AFM state is induced in  $\text{Fe}_4\text{GeTe}_2$  with Co substitution [24], and As substitution for Ge in  $\text{Fe}_3\text{GeTe}_2$  suppresses  $T_C$  [29]. Recently, a vdW intrinsic ferromagnetic crystal  $\text{Fe}_3\text{GaTe}_2$ , which has the same structure as  $\text{Fe}_3\text{GeTe}_2$ , was reported to exhibit record-high above-room-temperature Curie temperature ( $T_C \sim 350$ – $380$  K) for known layered vdW intrinsic ferromagnets [30]. The robust large perpendicular magnetic anisotropy (PMA) and high Curie temperature are beneficial for experimentally exploring magnetic properties down to the 2D limit. Therefore, it would be interesting to see how chemical substitution affects the physical properties of  $\text{Fe}_3\text{GaTe}_2$ .

In this work, we report the successful growth of high quality  $(\text{Fe}_{1-x}\text{Co}_x)_3\text{GaTe}_2$  single crystals with  $x = 0$ – $0.55$  and  $(\text{Fe}_{1-x}\text{Ni}_x)_3\text{GaTe}_2$  single crystals with  $x = 0$ – $0.46$ . A small amount of Co or Ni doping results in a significant increase of the coercive field ( $H_C$ ). Doping with Co or Ni suppresses the magnetic transition temperatures. In addition, Co doping tunes the crystals from ferromagnetism to antiferromagnetism and then to the spin-glass state, while Ni doping tunes the crystals from ferromagnetism to the spin-glass state.

**II. EXPERIMENTAL DETAILS**

High-quality  $(\text{Fe}_{1-x}\text{Co}_x)_3\text{GaTe}_2$  and  $(\text{Fe}_{1-x}\text{Ni}_x)_3\text{GaTe}_2$  single crystals were grown by the chemical vapor transport (CVT) method. High purity Fe powders (Aladdin, 99.95%), Co or Ni powders (Aladdin, 99.999%), Ga lumps (Aladdin, 99.999%), and Te powders (Aladdin, 99.999%) in the molar ratio of  $3 - x : x : 1 : 2$  and 5 mg/cm<sup>3</sup> iodine powder as vapor transport agent were mixed and loaded into 20-cm-long quartz

\*Corresponding author: leibin@ahu.edu.cn

†Corresponding author: chenxh@ustc.edu.cn

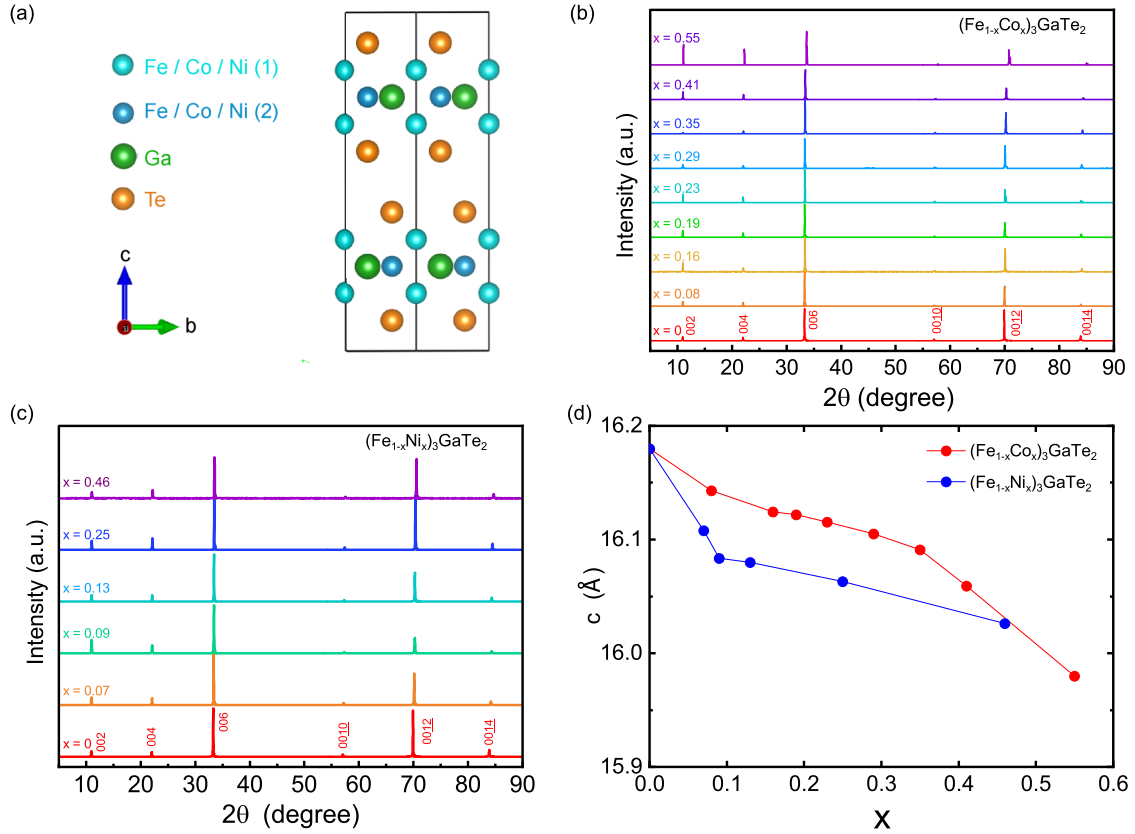


FIG. 1. (a) A schematic illustration of the crystal structure of  $(\text{Fe}_{1-x}\text{Co}_x)_3\text{GaTe}_2$  and  $(\text{Fe}_{1-x}\text{Ni}_x)_3\text{GaTe}_2$ . (b),(c) The single-crystalline XRD patterns of typical  $(\text{Fe}_{1-x}\text{Co}_x)_3\text{GaTe}_2$  and  $(\text{Fe}_{1-x}\text{Ni}_x)_3\text{GaTe}_2$  single crystals at room temperature. (d) Doping-dependent  $c$ -axis lattice parameters for  $(\text{Fe}_{1-x}\text{Co}_x)_3\text{GaTe}_2$  and  $(\text{Fe}_{1-x}\text{Ni}_x)_3\text{GaTe}_2$  at room temperature.

tubes. The sealed quartz tubes were put into a horizontal double-temperature-zone tube furnace with one end heated to  $825^\circ\text{C}$  and the other end at  $700^\circ\text{C}$  for 10 days, followed by slowly cooling down to room temperature. The shiny single crystals were obtained at the low temperature end of the tube furnace.

All single crystals were characterized using x-ray diffraction (XRD) (SmartLab-9, Rigaku Corp.) with  $\text{Cu } K_\alpha$  radiation and energy-dispersive x-ray spectroscopy (EDS). The direct current (DC) and alternating current (AC) magnetic susceptibility were measured on a magnetic property measurement system equipped with a vibrating sample magnetometer (MPMS-SQUID-VSM, Quantum Design), and the electric transport properties were measured by a physical property measurement system (PPMS DynaCool, Quantum Design).

### III. RESULTS AND DISCUSSION

#### A. Structure and composition

The platelike single-crystalline samples of  $(\text{Fe}_{1-x}\text{Co}_x)_3\text{GaTe}_2$  ( $0 \leq x \leq 0.55$ ) and  $(\text{Fe}_{1-x}\text{Ni}_x)_3\text{GaTe}_2$  ( $0 \leq x \leq 0.46$ ) with typical size of  $5 \times 5 \times 0.1\text{mm}^3$  were grown via a chemical vapor transport (CVT) method. The actual substitution levels ( $x$ ) and compositions were determined by EDS analysis (see Table S1 and Figs. S1 and S2 in the Supplemental Material [31]). Unlike the  $\text{Fe}_3\text{GeTe}_2$ ,  $\text{Fe}_3\text{GaTe}_2$  has almost no vacancies. Figure 1(a) illustrates the crystal structure of  $(\text{Fe}_{1-x}\text{Co}_x)_3\text{GaTe}_2$  and  $(\text{Fe}_{1-x}\text{Ni}_x)_3\text{GaTe}_2$ , which

is the same as  $\text{Fe}_3\text{GaTe}_2$  with a hexagonal structure (space group  $P6_3/mmc$ ). The  $(\text{Fe}_{1-x}\text{Co}_x)_3\text{Ga}$  or  $(\text{Fe}_{1-x}\text{Ni}_x)_3\text{Ga}$  plane is sandwiched between two Te layers along the  $c$  direction. The vdW gap between Te layers makes crystals cleavable. Note that there are two crystallographic Fe sites and both sites may be doped by Co or Ni. Figures 1(b) and 1(c) present the single-crystalline x-ray diffraction (XRD) patterns at room temperature for the  $(\text{Fe}_{1-x}\text{Co}_x)_3\text{GaTe}_2$  ( $0 \leq x \leq 0.55$ ) and  $(\text{Fe}_{1-x}\text{Ni}_x)_3\text{GaTe}_2$  ( $0 \leq x \leq 0.46$ ) single crystals, respectively. Pronounced  $(00l)$  diffraction peaks are observed. All diffraction peaks are well indexed and no additional peaks appear, suggesting that the Co or Ni doped single crystals maintain the original crystal structure. Additionally, powder XRD measurement was carried out for  $\text{Fe}_3\text{GaTe}_2$  parent compound, where all diffraction peaks are well indexed and no additional peaks appear (see Fig. S3 in the Supplemental Material [31]). It should be noted that the Rietveld refinement of the powder XRD is not possible due to the strong preferred orientation. The homogeneous distribution of Fe-Co or Fe-Ni atoms as presented in the EDS mapping indicates that Fe atoms are well replaced by Co or Ni dopants. Lattice parameters of the  $c$  axis ( $c$ ) estimated from Figs. 1(b) and 1(c) are plotted as a function of Co or Ni concentration, as shown in Fig. 1(d). The  $c$ -axis lattice parameter of the undoped compound is  $16.19 \text{ \AA}$ , consistent with previous reported results [30]. The lattice parameters decrease with increasing the Co or Ni doping level, which may be caused by the smaller ionic radius of doped ions.

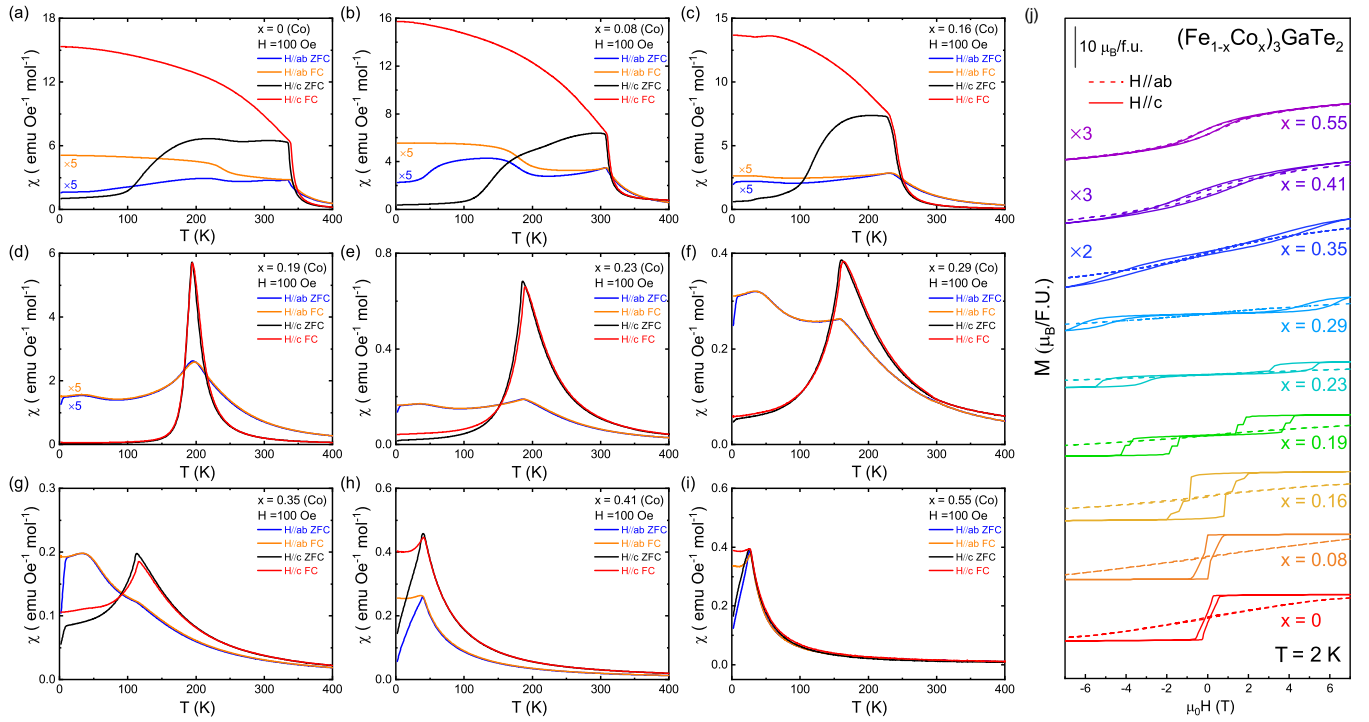


FIG. 2. (a)–(i) Temperature-dependent magnetic susceptibility measurements with zero-field-cooling and field-cooling conditions under an applied magnetic field  $H = 100$  Oe along the in-plane and out-of-plane directions for Co doped  $\text{Fe}_3\text{GaTe}_2$  crystals. (j)  $M(H)$  curves measured for  $(\text{Fe}_{1-x}\text{Co}_x)_3\text{GaTe}_2$  ( $0 \leq x \leq 0.55$ ) single crystals at  $T = 2$  K between  $-7$  T and  $7$  T. Solid and dashed lines are data for  $H//c$  and  $H//ab$ , respectively. These curves are shifted vertically for clarity.

### B. Magnetic properties

To track the systematic evolution of the magnetic properties in  $(\text{Fe}_{1-x}\text{Co}_x)_3\text{GaTe}_2$  single crystals with various Co doping level, we performed temperature-dependent magnetic susceptibility measurements with zero-field-cooling (ZFC) and field-cooling (FC) conditions under an applied magnetic field  $H = 100$  Oe along the in-plane and out-of-plane directions. In the lower doping range ( $0 \leq x \leq 0.16$ ), as depicted in Figs. 2(a)–2(c), the magnetic susceptibility (FC condition,  $H//c$ ) increases rapidly and then tends to saturation with decreasing temperature, suggesting a ferromagnetic transition. For  $x = 0$  [Fig. 2(a)],  $\text{Fe}_3\text{GaTe}_2$  shows ferromagnetism and  $T_C$  is about 349 K [see Fig. S4(a) in the Supplemental Material [31]]. The magnetic susceptibility for  $H//c$  is much larger than that of  $H//ab$ , indicating that the  $c$  axis is the easy-magnetization axis, which agrees with the previous work [30]. Considering the shape of the crystals, the demagnetization factor in the out-of-plane direction is much larger than that in the in-plane direction. After considering the demagnetization effect, it will not change the fact that the  $c$  axis is the easy-magnetization axis. The  $\chi$ - $T$  curves for the  $x = 0.16$  sample measured under ZFC and FC conditions are displayed in Fig. 2(c). An abrupt paramagnetic (PM) to FM transition at about 240 K has been observed [see Fig. S4(c) in the Supplemental Material [31]]. The  $T_C$  of the samples decreases with increase of Co-doped content, which may be attributed to the disorder effect caused by Co doping [21]. In the moderate doping range ( $0.19 \leq x \leq 0.35$ ), as presented in Figs. 2(d)–2(g), pronounced peaks are observed whether the magnetic field is applied within the  $ab$  plane or along the  $c$  axis, indicat-

ing an AFM-like transition. For the  $x = 0.19$  sample, the Néel temperature ( $T_N$ ) is about 195 K. As the doping concentration increases, the  $T_N$  of the crystals is suppressed. In the higher doping range ( $0.41 \leq x \leq 0.55$ ), as shown in Figs. 2(h) and 2(i), samples exhibit completely different magnetic susceptibility behavior. Figure 2(i) shows the  $\chi$ - $T$  curves for the  $x = 0.55$  sample, which exhibit peaks at  $T \sim 26$  K. We speculate that the sample may exhibit spin-glass behavior. To confirm this assumption, we carried out the frequency-dependent AC magnetic susceptibility measurements. As shown in Fig. 3(b), the temperature-dependent real part of AC magnetic susceptibility ( $\chi'_{ac}$ ) curves shows a peak at the low temperature and the peak shifts toward the higher temperature with increasing measuring frequency, suggesting a typical spin-glass state [32–34]. This result suggests that the magnetic ground state evolves from the AFM to the spin-glass state with further doping of Co.

Figure 2(j) displays the isothermal  $M(H)$  curves measured for  $(\text{Fe}_{1-x}\text{Co}_x)_3\text{GaTe}_2$  ( $0 \leq x \leq 0.55$ ) single crystals at  $T = 2$  K between  $-7$  T and  $7$  T. Solid and dashed lines are data for  $H//c$  and  $H//ab$ , respectively. In the lower doping range ( $0 \leq x \leq 0.16$ ), the  $M(H)$  curves show a near-rectangular feature, indicating a FM hysteresis loop of typical pinning-type ferromagnets.  $M$  saturates at relatively low magnetic field when the magnetic field is along the  $c$  axis, suggesting an out-of-plane magnetic anisotropy. In the moderate doping range ( $0.19 \leq x \leq 0.35$ ), for  $H//c$ , with increasing the magnetic field,  $M$  begins with a slow increase and then displays a sharp leap, eventually tending to saturation, suggesting a field-induced spin-flop transition and indicating that samples may host an A-type AFM structure [35,36], which

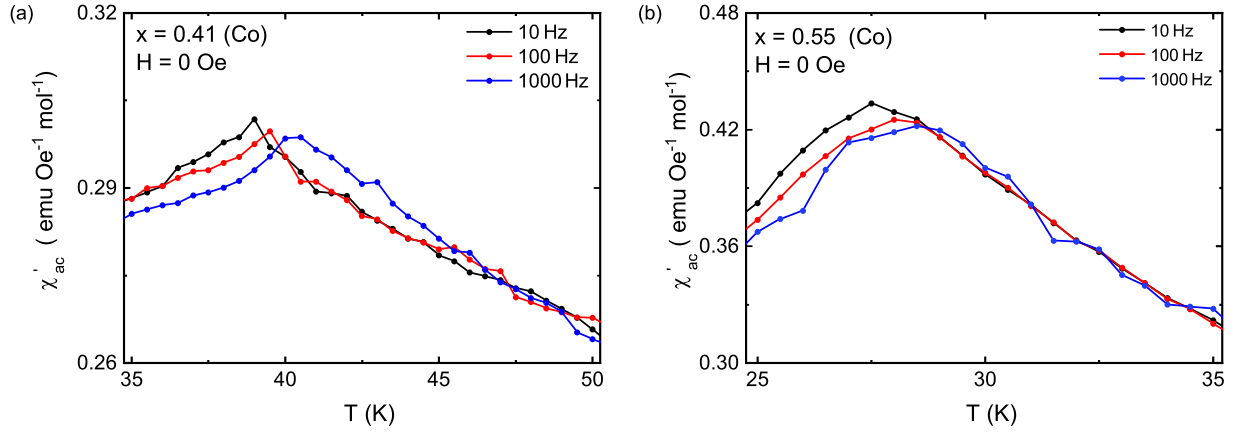


FIG. 3. The temperature-dependent real part of AC magnetic susceptibility ( $\chi'_{ac}$ ) for  $(\text{Fe}_{1-x}\text{Co}_x)_3\text{GaTe}_2$  single crystals with  $x = 0.41$  and  $x = 0.55$ , respectively. During the measurement at various frequencies, an AC field of 0 Oe is applied.

is consistent with the results obtained from the  $\chi$ - $T$  curves. The evolution of magnetic properties from  $x = 0$  to  $x = 0.35$  could be explained by a bilayer Stoner-Wohlfarth model based on two ferromagnetic layers with a uniaxial perpendicular anisotropy  $K$  and a weak antiferromagnetic exchange coupling  $J$  [37]. For  $(\text{Fe}_{1-x}\text{Co}_x)_3\text{GaTe}_2$  ( $0 \leq x \leq 0.16$ ) single crystals, the interlayer AFM exchange coupling is too weak to overcome the energy of magnetocrystalline anisotropy. Therefore, the crystals exhibit ferromagnetism and show ferromagnetic hysteresis at low temperature. With increasing the Co-doped level,  $J$  gradually increases and eventually drives the crystals from the FM state to the AFM state. With the further increase of Co doping content, the disorder effect evolves the sample to the spin-glass state.

As known from previous Ni-based layered tellurides that are exclusively Pauli paramagnets, nickel is nonmagnetic in this structure [38–40]. As a result, Ni substitution of Fe gives a fantastic chance to investigate the influence of dilution on the FM ground state in  $\text{Fe}_3\text{GaTe}_2$ . In this work, with Ni

substitution, the magnetic properties of the  $(\text{Fe}_{1-x}\text{Ni}_x)_3\text{GaTe}_2$  ( $0 \leq x \leq 0.46$ ) crystals change significantly. In the lower doping range ( $0 \leq x \leq 0.09$ ), as shown in Figs. 4(a)–4(c), the single crystals exhibit ferromagnetism. It is very obvious that the doping of Ni suppresses the ferromagnetic transition temperature from  $T_C \sim 349$  K ( $x = 0$ ) down to  $T_C \sim 161$  K ( $x = 0.09$ ) (see Fig. S5 in the Supplemental Material [31]). The suppression of  $T_C$  may be attributed to the disorder effect and magnetic dilution effect from the Ni substitution. In addition, an obvious hump feature in the  $\chi$ - $T$  curve has been observed for sample with  $x = 0.09$ . This phenomenon is also present in Co-doped  $\text{Fe}_3\text{GaTe}_2$  and it may be caused by a pinning-depinning crossover of magnetic domain walls [23]. In the higher doping range ( $0.13 \leq x \leq 0.46$ ), as shown in Figs. 4(d)–4(f), samples exhibit completely different magnetic susceptibility behavior. The  $\chi$ - $T$  curves for  $x = 0.46$  sample are shown in Fig. 4(f). The magnetic susceptibility increases rapidly and a peak at  $T \sim 38$  K has been observed, and then

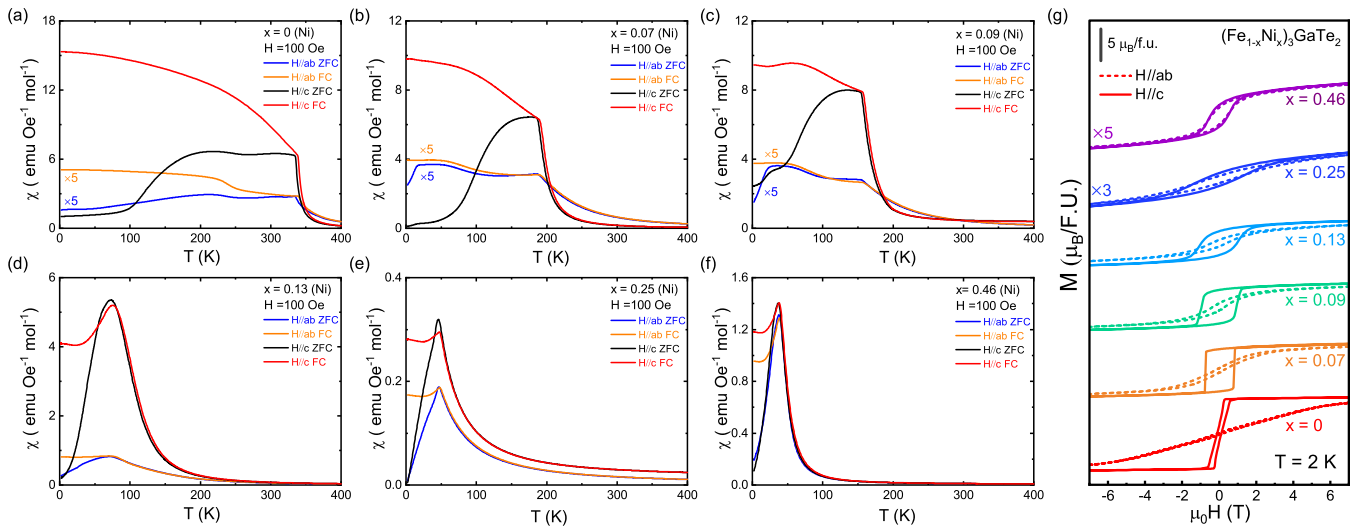


FIG. 4. (a)–(f) Temperature-dependent magnetic susceptibility measurements with zero-field-cooling and field-cooling conditions under an applied magnetic field  $H = 100$  Oe along the in-plane and out-of-plane directions for Ni doped  $\text{Fe}_3\text{GaTe}_2$  crystals. (g)  $M(H)$  curves measured for  $(\text{Fe}_{1-x}\text{Ni}_x)_3\text{GaTe}_2$  ( $0 \leq x \leq 0.46$ ) single crystals at  $T = 2$  K between  $-7$  T and  $7$  T. Solid and dashed lines are data for  $H//c$  and  $H//ab$ , respectively. These curves are shifted vertically for clarity.

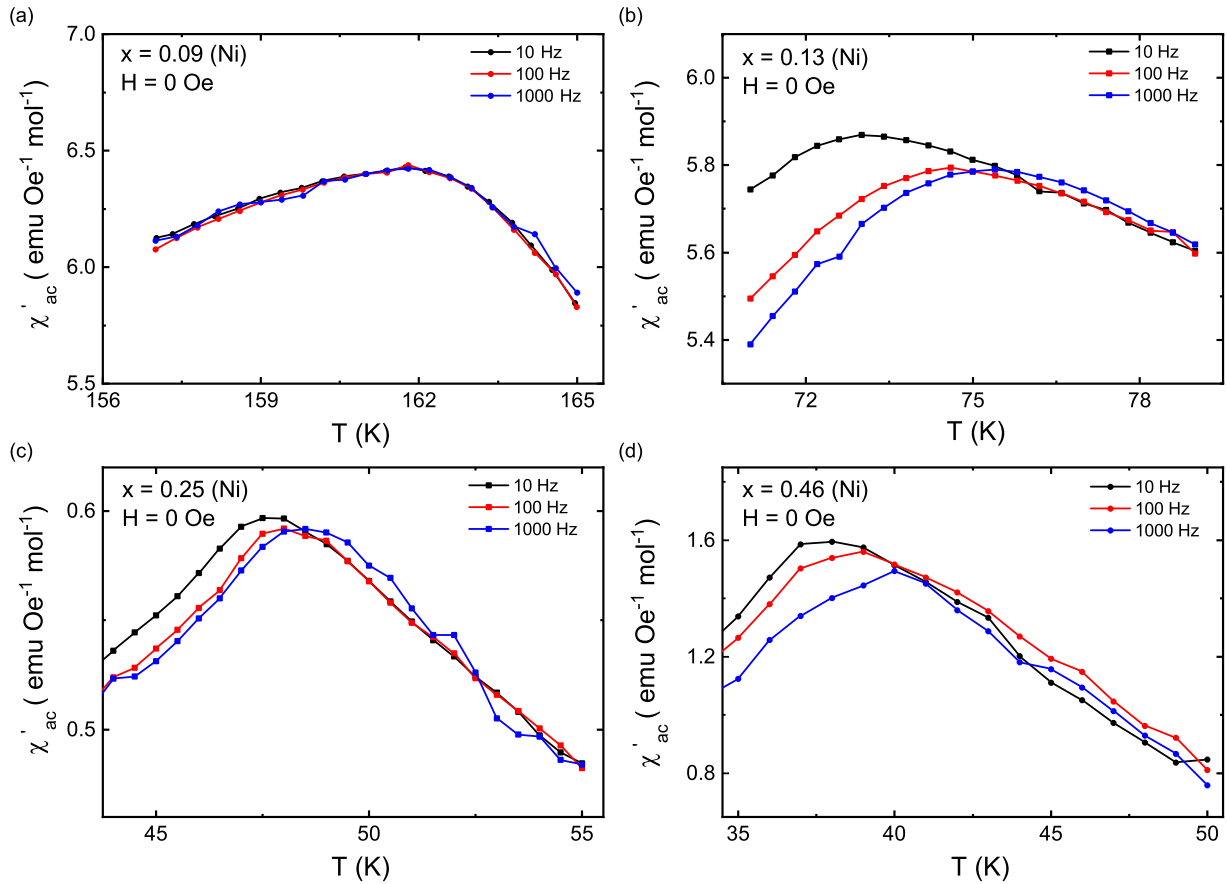


FIG. 5. The temperature-dependent real part of AC magnetic susceptibility ( $\chi'_{ac}$ ) for  $(\text{Fe}_{1-x}\text{Ni}_x)_3\text{GaTe}_2$  single crystals with  $x = 0.09$  to  $x = 0.46$ . During the measurement at various frequencies, an AC field of 0 Oe is applied.

the magnetic susceptibility gradually decreases with decreasing temperature. What is more, the FC curves separate with the ZFC curves at low temperature. The shape of the curves suggests that the sample may exhibit spin-glass behavior. To confirm this assumption, the frequency-dependent AC magnetic susceptibility was also carried out. As shown in Fig. 5(a), the  $\chi'_{ac}$ - $T$  curve for the  $x = 0.09$  sample shows a peak and the peak position is almost unchanged under various frequencies, indicating that the sample is still in the ferromagnetic state. As shown in Figs. 5(b)–5(d), the  $\chi'_{ac}$ - $T$  curves for  $x \geq 0.13$  samples show peaks at the low temperature and the peaks shift toward the higher temperature with increasing measuring frequency, suggesting a typical spin-glass state [32–34]. The evolution from the FM to the spin-glass state with further doping of Ni may originate from the structural disorder and Fe deficiency caused by nickel doping [21].

Figure 4(g) displays the isothermal  $M(H)$  curves measured for  $(\text{Fe}_{1-x}\text{Ni}_x)_3\text{GaTe}_2$  ( $0 \leq x \leq 0.46$ ) single crystals at  $T = 2$  K between  $-7$  T and  $7$  T. Solid and dashed lines are data for  $H//c$  and  $H//ab$ , respectively. In the lower doping range ( $0 \leq x \leq 0.09$ ), the  $M(H)$  curves show a near-rectangular feature, suggesting that samples are pinning-type ferromagnets. The magnetic remanence to saturated magnetization ratio ( $M_R/M_S$ ) at  $T = 2$  K is plotted in Fig. S6 (Supplemental Material [31]). The value of  $M_R/M_S$  is very low for  $\text{Fe}_3\text{GaTe}_2$  single crystals ( $M_R/M_S \sim 0.2$ ), however a little amount of Ni

doping generates a significant increase of the  $M_R/M_S$  value. For  $x = 0.07$ , the  $M_R/M_S$  ratio increases to 0.9. The samples with  $x = 0.07$  and  $x = 0.09$  present well-defined hard magnetic characteristics, similar to previously reported  $\text{Fe}_N\text{GeTe}_2$  few layer flakes [11,15,20]. These results imply that Ni doping also creates hard magnetic phases in bulk materials. With further increase of Ni doping content ( $x \geq 0.13$ ), the pinning-type magnetic features are gradually weakened, showing a typical hysteresis loop of the spin-glass state.

It should be pointed out that  $H_C$  has largely improved with the increase of doping level at  $T = 2$  K. As shown in Figs. 6(a) and 6(b),  $H_C$  increases from 0.9 KOe ( $x = 0$ ) to 7.8 KOe ( $x = 0.16$ ) for  $(\text{Fe}_{1-x}\text{Co}_x)_3\text{GaTe}_2$  single crystals and increases to 9.4 KOe ( $x = 0.09$ ) for  $(\text{Fe}_{1-x}\text{Ni}_x)_3\text{GaTe}_2$  single crystals. Generally speaking, coercivity occurs as a result of both the magnetocrystalline anisotropy and the domain pinning in the material. To clearly address the two effects, the anisotropy energy ( $K_u$ ) has been estimated by the formula  $K_u = H_K M_{\text{sat}}/2$ , where  $H_K$  is the anisotropy field and  $M_{\text{sat}}$  is the saturation magnetization. We have extracted the  $H_K$  and  $M_{\text{sat}}$  values of  $(\text{Fe}_{1-x}\text{Co}_x)_3\text{GaTe}_2$  with  $x = 0 - 0.16$  from Fig. 2(j) and  $(\text{Fe}_{1-x}\text{Ni}_x)_3\text{GaTe}_2$  with  $x = 0 - 0.09$  from Fig. 4(g). As shown in Figs. 6(c) and 6(d),  $K_u$  dramatically decreases with increasing  $x$  and thus cannot enhance the  $H_C$ . Based on this result, we attribute the enhancement of  $H_C$  to the increase of domain pinning effect induced by Co or Ni doping. A major source of hysteresis in ferromagnets is the pinning of

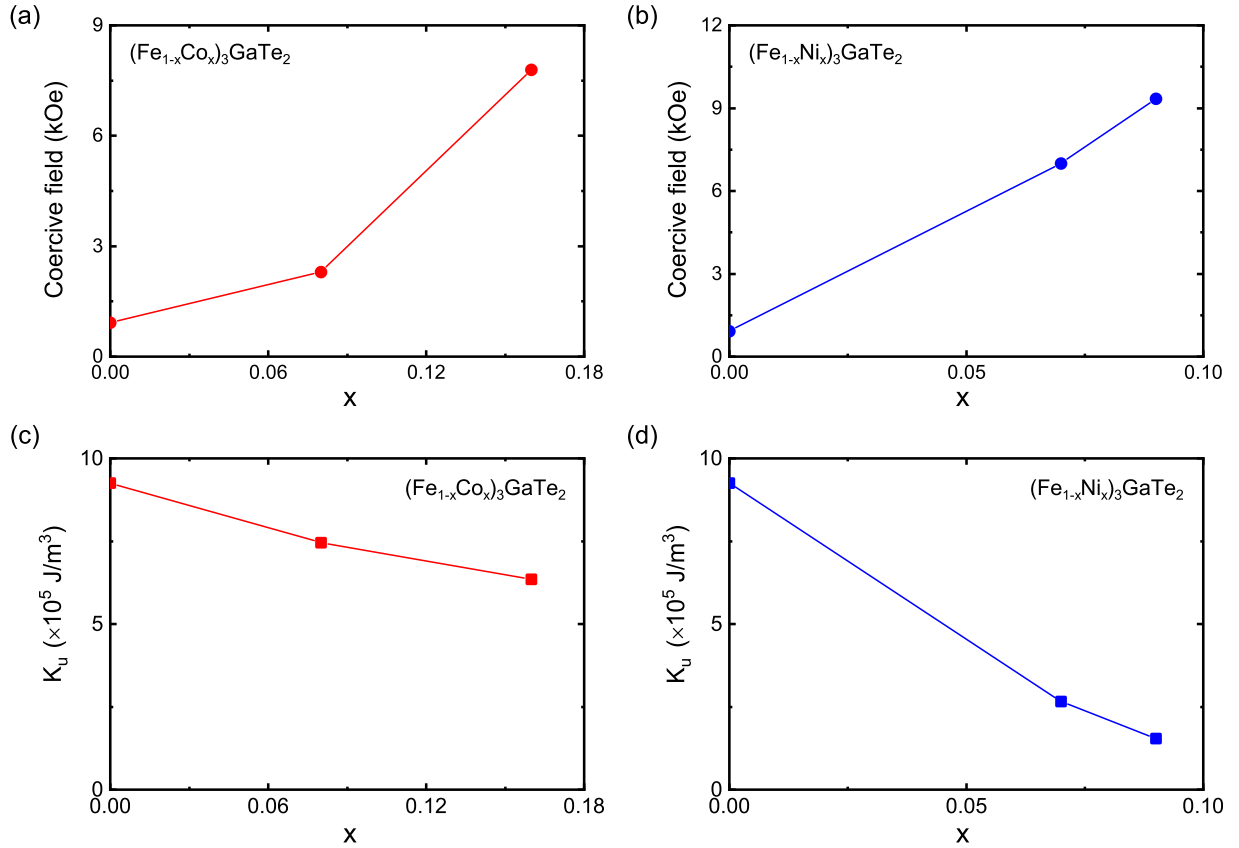


FIG. 6. (a),(b) Doping level dependence of the coercive fields for  $(\text{Fe}_{1-x}\text{Co}_x)_3\text{GaTe}_2$  ( $0 \leq x \leq 0.16$ ) and  $(\text{Fe}_{1-x}\text{Ni}_x)_3\text{GaTe}_2$  ( $0 \leq x \leq 0.09$ ) single crystals, respectively. (c),(d) Doping level dependence of the anisotropy energy ( $K_u$ ) for  $(\text{Fe}_{1-x}\text{Co}_x)_3\text{GaTe}_2$  ( $0 \leq x \leq 0.16$ ) and  $(\text{Fe}_{1-x}\text{Ni}_x)_3\text{GaTe}_2$  ( $0 \leq x \leq 0.09$ ) single crystals, respectively. All data are calculated from Figs. 2(j) and 4(g).

magnetic domain walls. To achieve a high  $H_C$  in pinning-type magnets, the formation of a large domain wall energy (DWE) and an effective network of pinning centers capable of locally increasing DWE to inhibit the domain wall movement is essential [41]. The doping of Co or Ni should somehow greatly improve the DWE of  $\text{Fe}_3\text{GaTe}_2$  thus inducing hard magnetic properties.

### C. Transport properties

Figures 7 and 8 display the temperature-dependent in-plane resistivity for the  $(\text{Fe}_{1-x}\text{Co}_x)_3\text{GaTe}_2$  ( $0 \leq x \leq 0.55$ ) and  $(\text{Fe}_{1-x}\text{Ni}_x)_3\text{GaTe}_2$  ( $0 \leq x \leq 0.46$ ) single crystals, respectively. At  $T \sim 348 \text{ K}$ , a kink can be seen in the  $\rho$ - $T$  curve of the  $\text{Fe}_3\text{GaTe}_2$ , consistent with the magnetic transition observed in the magnetic susceptibility measurement. Additionally, similar kinks have been observed in all lowly doped samples with  $x = 0 - 0.35$  for  $(\text{Fe}_{1-x}\text{Co}_x)_3\text{GaTe}_2$  and  $x = 0 - 0.09$  for  $(\text{Fe}_{1-x}\text{Ni}_x)_3\text{GaTe}_2$ . The blue arrows denote the magnetic transition temperature ( $T_C$  or  $T_N$ ), which correspond to the peaks observed from the derivative of the  $\rho$ - $T$  curves (see Figs. S7 and S8 in the Supplemental Material [31]). It is obvious that Co doping reduces the magnetic transition temperature from  $T_C \sim 348 \text{ K}$  ( $x = 0$ ) down to  $T_N \sim 114 \text{ K}$  ( $x = 0.35$ ), and Ni doping drops  $T_C$  to about  $156 \text{ K}$  ( $x = 0.09$ ). As mentioned above, the suppression of magnetic transition temperatures may be attributed to the

doping-induced disorder effect, which may also be confirmed by the resistivity measurements. The parent  $\text{Fe}_3\text{GaTe}_2$  crystal exhibits metallic behavior at high temperature and presents the up-turn feature in the resistance at low temperature [30]. Higher doped samples ( $x = 0.41 - 0.55$  in Co doped or  $x = 0.13 - 0.46$  in Ni doped) show semiconductorlike behavior at low temperature, and the corresponding magnetic transition signal disappears. Moreover, for Ni doped samples, the up-turn feature at low temperature becomes more obvious. Especially the  $(\text{Fe}_{0.54}\text{Ni}_{0.46})_3\text{GaTe}_2$  sample almost exhibits semiconductor behavior throughout the entire measured temperature range. A possible interpretation is that disorders induced by doping cause the localization of carriers. The realization of a spin-glass state in highly doped  $\text{Fe}_3\text{GaTe}_2$  is because of the strong disorder effect, in accordance with the absence of peaks observed in the derivative of the  $\rho$ - $T$  curves.

Figures 9 and 10 present the temperature-dependent Hall resistance  $R_{xy}(H)$  measured for  $(\text{Fe}_{1-x}\text{Co}_x)_3\text{GaTe}_2$  ( $0 \leq x \leq 0.55$ ) and  $(\text{Fe}_{1-x}\text{Ni}_x)_3\text{GaTe}_2$  ( $0 \leq x \leq 0.46$ ) single crystals, respectively. At  $T = 2 \text{ K}$ , the  $R_{xy}(H)$  curves generally track the  $M(H)$  curves. For the lower doping samples ( $0 \leq x \leq 0.16$  for  $(\text{Fe}_{1-x}\text{Co}_x)_3\text{GaTe}_2$  and  $0 \leq x \leq 0.09$  for  $(\text{Fe}_{1-x}\text{Ni}_x)_3\text{GaTe}_2$ ), the  $R_{xy}(H)$  curves show obvious anomalous Hall effect (AHE) at low temperature. As the temperature increases, the AHE gradually shrinks and the  $R_{xy}(H)$  curves finally turn into

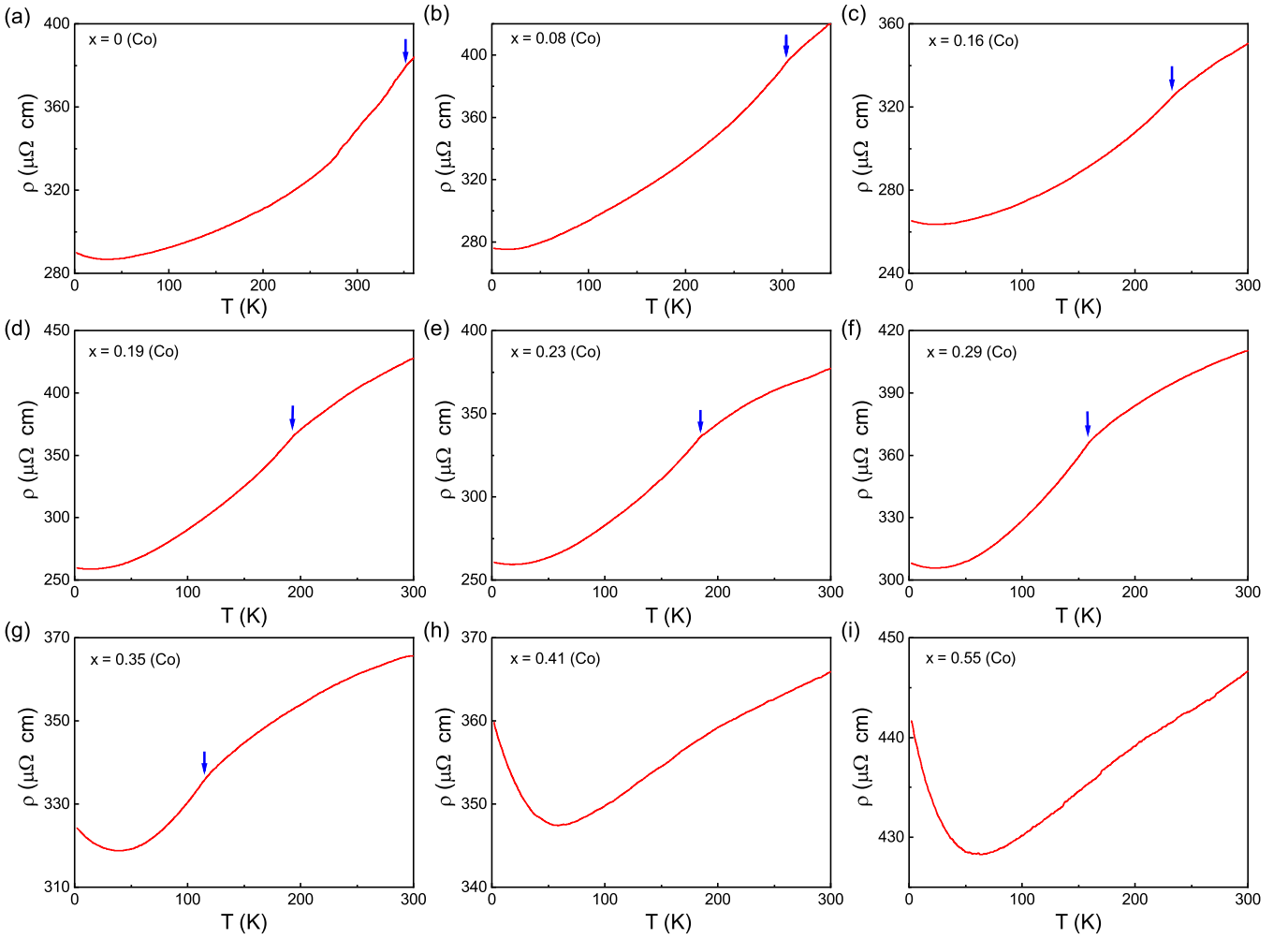


FIG. 7. Temperature-dependent in-plane resistivity for  $(\text{Fe}_{1-x}\text{Co}_x)_3\text{GaTe}_2$  ( $0 \leq x \leq 0.55$ ) single crystals. The blue arrows denote the magnetic transition temperature ( $T_C$  or  $T_N$ ), which decreases with increasing the doping level of Co.

straight lines. In the moderate doping range ( $0.19 \leq x \leq 0.35$  for  $(\text{Fe}_{1-x}\text{Co}_x)_3\text{GaTe}_2$ ), the spin-flop transitions gradually disappear as the temperature increases, and then nonlinear behaviors are observed across a wide range of temperature. Compared to the square-shaped hysteresis of AHE in the lower doping samples, a narrow and tilted hysteresis loop shows up for the higher doping samples [ $0.41 \leq x \leq 0.55$  for  $(\text{Fe}_{1-x}\text{Co}_x)_3\text{GaTe}_2$  and  $0.13 \leq x \leq 0.46$  for  $(\text{Fe}_{1-x}\text{Ni}_x)_3\text{GaTe}_2$ ]. As the temperature increases, the  $R_{xy}(H)$  curves gradually turn into straight lines. Hence, we can define the temperature at which the nonlinear feature of the  $R_{xy}(H)$  curves disappears as the magnetic transition temperature ( $T_C$  or  $T_N$ ).

It should be pointed out that the  $T_C$  or  $T_N$  taken from magnetic susceptibility measurements, resistivity measurements, and Hall measurements agrees within uncertainty, which is clearly visible in the phase diagrams. As shown in Fig. S9, we have also estimated the carrier density ( $n_e$ ) at  $T = 2$  K for  $(\text{Fe}_{1-x}\text{Co}_x)_3\text{GaTe}_2$  ( $0 \leq x \leq 0.35$ ) and  $(\text{Fe}_{1-x}\text{Ni}_x)_3\text{GaTe}_2$  ( $0 \leq x \leq 0.09$ ). Obviously,  $n_e$  decreases with increasing doping level, which implies that doping by Co or Ni can lead to localization of charge carriers in  $\text{Fe}_3\text{GaTe}_2$ .

#### D. Phase diagrams

Based on the transport and magnetic measurements, the phase diagrams of the Co or Ni doped  $\text{Fe}_3\text{GaTe}_2$  crystals are plotted in Fig. 11. The magnetic transition temperatures of  $(\text{Fe}_{1-x}\text{Co}_x)_3\text{GaTe}_2$  ( $0 \leq x \leq 0.55$ ) and  $(\text{Fe}_{1-x}\text{Ni}_x)_3\text{GaTe}_2$  ( $0 \leq x \leq 0.46$ ) single crystals are extracted from magnetic susceptibility measurements ( $T_M$ , red circles), resistivity measurements ( $T_R$ , black stars), and Hall measurements ( $T_H$ , blue squares). As shown in Fig. 11(a), Co doping in  $\text{Fe}_3\text{GaTe}_2$  tunes the crystals from ferromagnetism to antiferromagnetism and then to the spin-glass state. What is more, the magnetic transition temperatures are gradually suppressed upon Co doping. From a chemical standpoint, Co substitution is likely to change the intralayer local configuration and interlayer stacking arrangement of  $\text{Fe}_3\text{GaTe}_2$  crystals, which enables astonishing control of the magnetic response. As a result, our results demonstrate the sensitivity of magnetism in  $\text{Fe}_3\text{GaTe}_2$  to composition, and point out the significance of order-disorder in cleavable 2D magnetic materials. Meanwhile, we also provide clues and potential methods to manipulate the magnetic transition between FM and AFM states for  $(\text{Fe}_{1-x}\text{Co}_x)_3\text{GaTe}_2$  crystals. These findings hold promise

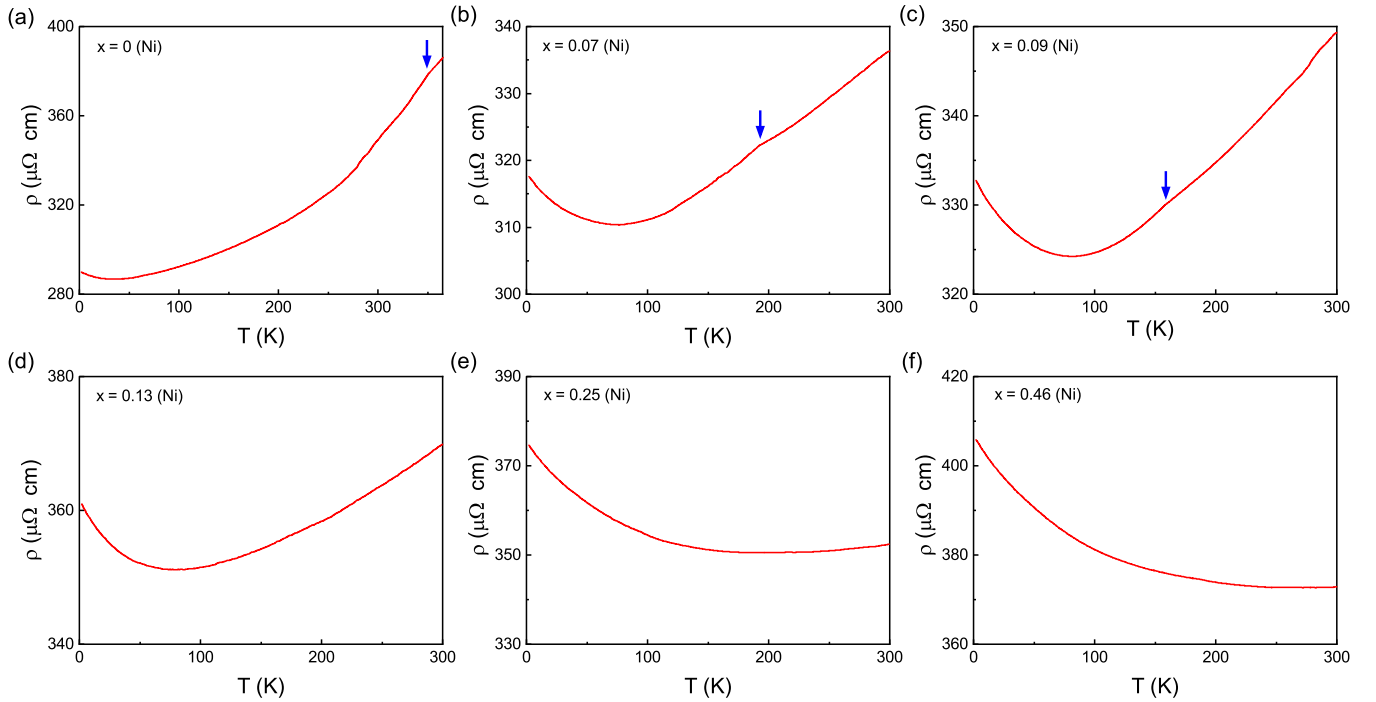


FIG. 8. Temperature-dependent in-plane resistivity for  $(\text{Fe}_{1-x}\text{Ni}_x)_3\text{GaTe}_2$  ( $0 \leq x \leq 0.46$ ) single crystals. The blue arrows denote the magnetic transition temperature ( $T_C$ ), which decreases with increasing the doping level of Ni.

for future advancements in magnetic data recording and information processing. As shown in Fig. 11(b), Ni doping in  $\text{Fe}_3\text{GaTe}_2$  tunes the crystals from ferromagnetism to the spin-glass state. The same as the situation with Co doping, the magnetic transition temperatures are gradually suppressed upon Ni doping. It should be emphasized that  $H_C$  increases to

2.3 kOe at  $T = 2$  K and  $T_C$  is approximately 309 K in Co doped  $\text{Fe}_3\text{GaTe}_2$  crystals with  $x = 0.08$ . Hard magnetism is essential for the application of two-dimensional magnetic materials in spintronic devices, and our experimental results provide fresh ideas for the application of  $\text{Fe}_3\text{GaTe}_2$ . Obviously, the doping effect of Co is different from that of Ni, especially the

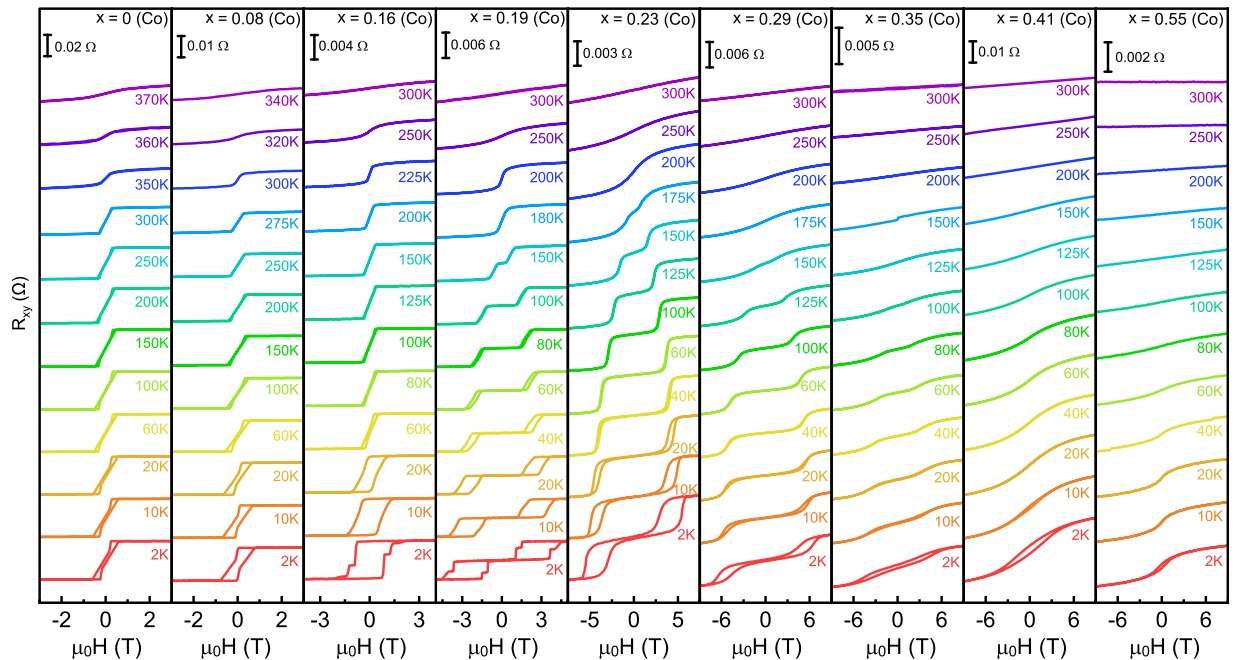


FIG. 9. Temperature-dependent Hall resistance [ $R_{xy}(H)$ ] for  $(\text{Fe}_{1-x}\text{Co}_x)_3\text{GaTe}_2$  single crystals with different Co doping. The  $R_{xy}(H)$  curves are shifted vertically for clarity. An obvious anomalous Hall effect is observed at low temperature for all samples. With increasing the doping level, the temperature at which the anomalous Hall effect disappears gradually decreases, suggesting the decrease of the magnetic transition temperature.



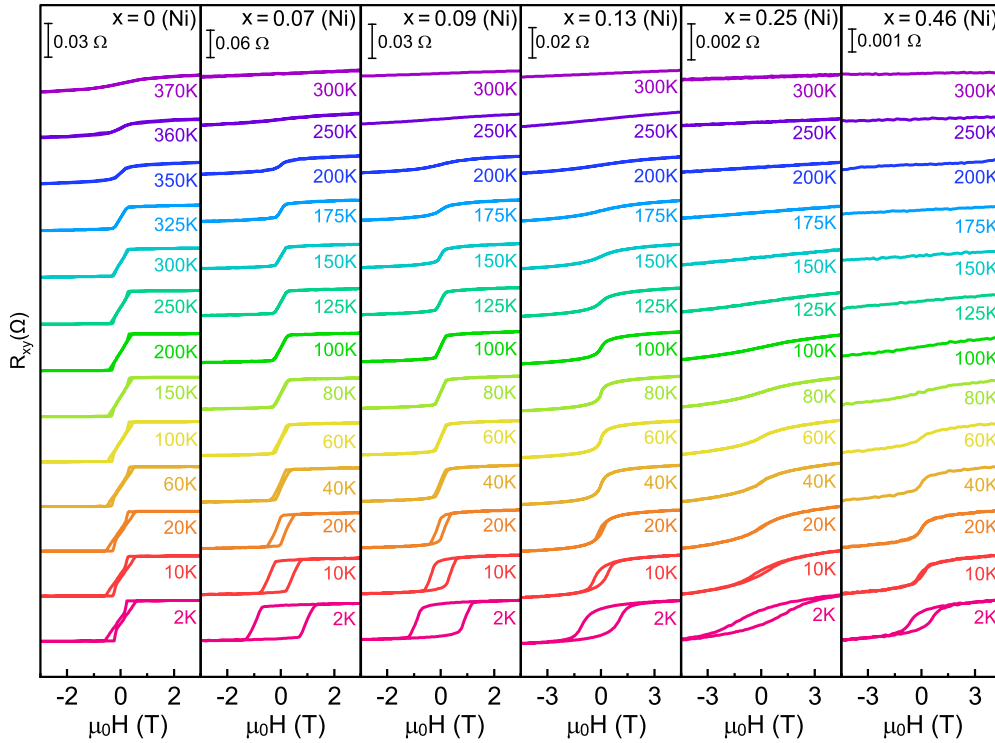


FIG. 10. Temperature-dependent Hall resistance [ $R_{xy}(H)$ ] for  $(\text{Fe}_{1-x}\text{Ni}_x)_3\text{GaTe}_2$  single crystals with different Ni doping. The  $R_{xy}(H)$  curves are shifted vertically for clarity. An obvious anomalous Hall effect is observed at low temperature for all samples. With increasing the doping level, the temperature at which the anomalous Hall effect disappears gradually decreases, suggesting the decrease of the magnetic transition temperature.

appearance of AFM states, making us believe that Co may have a moment in  $\text{Fe}_3\text{GaTe}_2$ .

#### IV. CONCLUSION

In summary, a series of  $(\text{Fe}_{1-x}\text{Co}_x)_3\text{GaTe}_2$  ( $0 \leq x \leq 0.55$ ) and  $(\text{Fe}_{1-x}\text{Ni}_x)_3\text{GaTe}_2$  ( $0 \leq x \leq 0.46$ ) single crystals have been successfully synthesized by CVT methods. The magnetic transition temperatures of  $\text{Fe}_3\text{GaTe}_2$  gradually decrease upon Co or Ni doping. In particular, Co doping tunes the crystals from ferromagnetism to antiferromagnetism and then

to the spin-glass state, while Ni doping tunes the crystals from ferromagnetism to spin-glass state. What is more, samples with lower doping level still maintain ferromagnetism, and the coercive fields and the values of magnetic remanence to saturated magnetization ratio are strongly doping dependent. Instead of making few layer samples, the hard magnetic properties have been realized in bulk single crystals of  $\text{Fe}_3\text{GaTe}_2$  with Co or Ni doping. The strong doping-dependent magnetic properties suggest that  $\text{Fe}_3\text{GaTe}_2$  has great potential for spintronic applications.

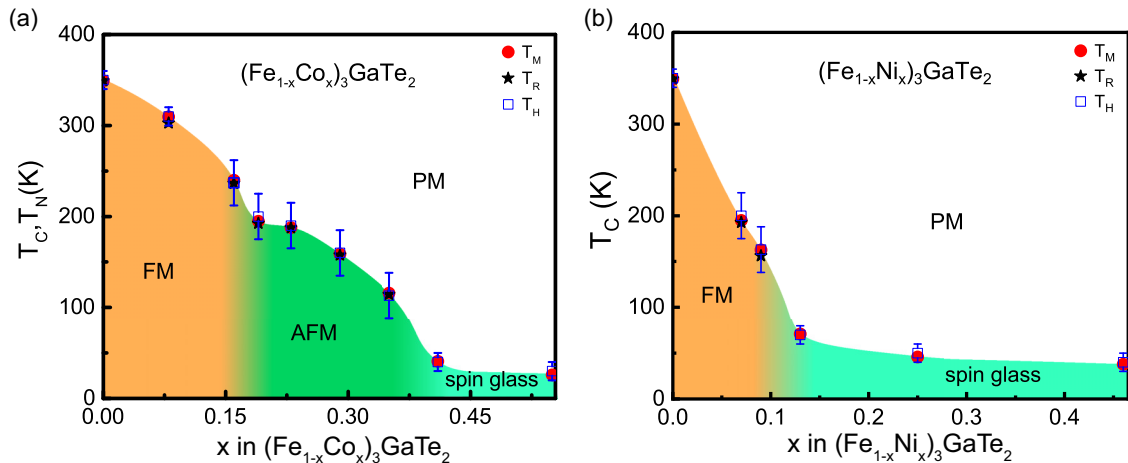


FIG. 11. (a) Magnetic phase diagram as a function of Co doping level for  $(\text{Fe}_{1-x}\text{Co}_x)_3\text{GaTe}_2$  ( $0 \leq x \leq 0.55$ ) single crystals. (b) Phase diagram of  $(\text{Fe}_{1-x}\text{Ni}_x)_3\text{GaTe}_2$  ( $0 \leq x \leq 0.46$ ) single crystals. The magnetic transition temperatures are extracted from magnetic susceptibility measurements ( $T_M$ , red circles), resistivity measurements ( $T_R$ , black stars), and Hall measurements ( $T_H$ , blue squares).

*Note added.* Recently, an article reporting similar changes in the magnetization of  $\text{Fe}_3\text{GaTe}_2$  upon Ni substitution was published [42].

### ACKNOWLEDGMENTS

This work was supported by the National Natural Science Foundation of China (Grants No. 11888101 and No.

12004365), the National Key Research and Development Program of the Ministry of Science and Technology of China (Grant No. 2022YFA1602601), the Strategic Priority Research Program of the Chinese Academy of Sciences (Grant No. XDB25000000), the Innovation Program for Quantum Science and Technology (Grant No. 2021ZD0302802), and the Anhui Initiative in Quantum Information Technologies (Grant No. AHY160000).

- [1] K. S. Novoselov, A. K. Geim, S. V. Morozov, D. Jiang, Y. Zhang, S. V. Dubonos, I. V. Grigorieva, and A. A. Firsov, Electric field effect in atomically thin carbon films, *Science* **306**, 666 (2004).
- [2] Q.-Y. Wang, Z. Li, W.-H. Zhang, Z.-C. Zhang, J.-S. Zhang, W. Li, H. Ding, Y.-B. Ou, P. Deng, K. Chang, J. Wen, C.-L. Song, K. He, J.-F. Jia, S.-H. Ji, Y.-Y. Wang, L.-L. Wang, X. Chen, X.-C. Ma, and Q.-K. Xue, Interface-induced high-temperature superconductivity in single unit-cell  $\text{FeSe}$  films on  $\text{SrTiO}_3$ , *Chin. Phys. Lett.* **29**, 037402 (2012).
- [3] Y. J. Yu, L. G. Ma, P. Cai, R. D. Zhong, C. Ye, J. Shen, G. D. Gu, X. H. Chen, and Y. B. Zhang, High-temperature superconductivity in monolayer  $\text{Bi}_2\text{Sr}_2\text{CaCu}_2\text{O}_{8+\delta}$ , *Nature (London)* **575**, 156 (2019).
- [4] B. Radisavljevic, A. Radenovic, J. Brivio, V. Giacometti, and A. Kis, Single-layer  $\text{MoS}_2$  transistors, *Nat. Nanotechnol.* **6**, 147 (2011).
- [5] L. K. Li, Y. J. Yu, G. J. Ye, Q. Q. Ge, X. D. Ou, H. Wu, D. L. Feng, X. H. Chen, and Y. B. Zhang, Black phosphorus field-effect transistors, *Nat. Nanotechnol.* **9**, 372 (2014).
- [6] Z. Fei, W. Zhao, T. A. Palomaki, B. Sun, M. K. Miller, Z. Zhao, J. Yan, X. D. Xu, and D. H. Cobden, Ferroelectric switching of a two-dimensional metal, *Nature (London)* **560**, 336 (2018).
- [7] J. M. Lu, O. Zheiliuk, I. Leermakers, N. F. Q. Yuan, U. Zeitler, K. T. Law, and J. T. Ye, Evidence for two-dimensional Ising superconductivity in gated  $\text{MoS}_2$ , *Science* **350**, 1353 (2015).
- [8] Y. Saito, Y. Kasahara, J. T. Ye, Y. Iwasa, and T. Nojima, Metallic ground state in an ion-gated two-dimensional superconductor, *Science* **350**, 409 (2015).
- [9] B. Huang, G. Clark, E. Navarro-Moratalla, D. R. Klein, R. Cheng, K. L. Seyler, D. Zhong, E. Schmidgall, M. A. McGuire, D. H. Cobden, W. Yao, D. Xiao, P. Jarillo Herrero, and X. Xu, Layer-dependent ferromagnetism in a van der Waals crystal down to the monolayer limit, *Nature (London)* **546**, 270 (2017).
- [10] C. Gong, L. Li, Z. Li, H. Ji, A. Stern, Y. Xia, T. Cao, W. Bao, C. Wang, Y. Wang, Z. Q. Qiu, R. J. Cava, S. G. Louie, J. Xia, and X. Zhang, Discovery of intrinsic ferromagnetism in two-dimensional van der Waals crystals, *Nature (London)* **546**, 265 (2017).
- [11] Y. Deng, Y. Yu, Y. Song, J. Zhang, N. Z. Wang, Z. Sun, Y. Yi, Y. Z. Wu, S. Wu, J. Zhu, J. Wang, X. H. Chen, and Y. B. Zhang, Gate-tunable room-temperature ferromagnetism in two-dimensional  $\text{Fe}_3\text{GeTe}_2$ , *Nature (London)* **563**, 94 (2018).
- [12] Z. Fei, B. Huang, P. Malinowski, W. Wang, T. Song, J. Sanchez, W. Yao, D. Xiao, X. Zhu, A. F. May, W. Wu, D. H. Cobden, J. H. Chu, and X. Xu, Two-dimensional itinerant ferromagnetism in atomically thin  $\text{Fe}_3\text{GeTe}_2$ , *Nat. Mater.* **17**, 778 (2018).
- [13] K. Kim, J. Seo, E. Lee, K.-T. Ko, B. S. Kim, B. G. Jang, J. M. Ok, J. Lee, Y. J. Jo, W. Kang, J. H. Shim, C. Kim, H. W. Yeom, B. Il Min, B. J. Yang, and J. S. Kim, Large anomalous Hall current induced by topological nodal lines in a ferromagnetic van der Waals semimetal, *Nat. Mater.* **17**, 794 (2018).
- [14] Y. Zhang, H. Lu, X. Zhu, S. Tan, W. Feng, Q. Liu, W. Zhang, Q. Chen, Y. Liu, X. Luo, D. Xie, L. Luo, Z. Zhang, and X. Lai, Emergence of Kondo lattice behavior in a van der Waals itinerant ferromagnet,  $\text{Fe}_3\text{GeTe}_2$ , *Sci. Adv.* **4**, eaao6791 (2018).
- [15] C. Tan, J. Lee, S. G. Jung, T. Park, S. Albarakati, J. Partridge, M. R. Field, D. G. McCulloch, L. Wang, and C. Lee, Hard magnetic properties in nanoflake van der Waals  $\text{Fe}_3\text{GeTe}_2$ , *Nat. Commun.* **9**, 1554 (2018).
- [16] J. Seo, D. Y. Kim, E. S. An, K. Kim, G.-Y. Kim, S.-Y. Hwang, D. W. Kim, B. G. Jang, H. Kim, G. Eom, S. Y. Seo, R. Stania, M. Muntwiler, J. Lee, K. Watanabe, T. Taniguchi, Y. J. Jo, J. Lee, B. I. Min, M. H. Jo *et al.*, Nearly room temperature ferromagnetism in a magnetic metal-rich van der Waals metal, *Sci. Adv.* **6**, eaay8912 (2020).
- [17] A. F. May, D. Ovchinnikov, Q. Zheng, R. Hermann, S. Calder, B. Huang, Z. Fei, Y. Liu, X. Xu, and M. A. McGuire, Ferromagnetism near room temperature in the cleavable van der Waals crystal  $\text{Fe}_5\text{GeTe}_2$ , *ACS Nano* **13**, 4436 (2019).
- [18] A. F. May, C. A. Bridges, and M. A. McGuire, Physical properties and thermal stability of  $\text{Fe}_{5-x}\text{GeTe}_2$  single crystals, *Phys. Rev. Mater.* **3**, 104401 (2019).
- [19] H. Zhang, R. Chen, K. Zhai, X. Chen, L. Caretta, X. Huang, R. V. Chopdekar, J. Cao, J. Sun, J. Yao, R. Birgeneau, and R. Ramesh, Itinerant ferromagnetism in van der Waals  $\text{Fe}_{5-x}\text{GeTe}_2$  crystals above room temperature, *Phys. Rev. B* **102**, 064417 (2020).
- [20] Y. Z. Deng, Z. J. Xiang, B. Lei, K. J. Zhu, H. M. Mu, W. Z. Zhuo, X. Y. Hua, M. J. Wang, Z. F. Wang, G. P. Wang, M. L. Tian, and X. H. Chen, Layer-number-dependent magnetism and anomalous Hall effect in van der Waals ferromagnet  $\text{Fe}_5\text{GeTe}_2$ , *Nano Lett.* **22**, 9839 (2022).
- [21] G. Drachuck, Z. Salman, M. W. Masters, V. Taufour, T. N. Lamichhane, Q. Lin, W. E. Straszheim, S. L. Bud'ko, and P. C. Canfield, Effect of nickel substitution on magnetism in the layered van der Waals ferromagnet  $\text{Fe}_3\text{GeTe}_2$ , *Phys. Rev. B* **98**, 144434 (2018).
- [22] X. Chen, Y. T. Shao, R. Chen, S. Susarla, T. Hogan, Y. He, H. Zhang, S. Wang, J. Yao, P. Ercius, D. A. Muller, R. Ramesh, and R. J. Birgeneau, Pervasive beyond room-temperature ferromagnetism in a doped van der Waals magnet, *Phys. Rev. Lett.* **128**, 217203 (2022).
- [23] C. K. Tian, C. Wang, W. Ji, J. C. Wang, T. L. Xia, L. Wang, J. J. Liu, H.-X. Zhang, and P. Cheng, Domain wall pinning and hard magnetic phase in Co-doped bulk single crystalline  $\text{Fe}_3\text{GeTe}_2$ , *Phys. Rev. B* **99**, 184428 (2019).
- [24] J. Seo, E. S. An, T. Park, S.-Y. Hwang, G.-Y. Kim, K. Song, W.-S. Noh, J. Y. Kim, G. S. Choi, M. Choi, E. Oh, K. Watanabe, T. Taniguchi, J. H. Park, Y. J. Jo, H. W. Yeom, S.-Y. Choi,

- J. H. Shim, and J. S. Kim, Tunable high-temperature itinerant antiferromagnetism in a van der Waals magnet, *Nat. Commun.* **12**, 2844 (2021).
- [25] J. C. Tian, F. Pan, S. Xu, K. Ai, T. Xia, and P. Cheng, Tunable magnetic properties in van der Waals crystals  $(\text{Fe}_{1-x}\text{Co}_x)_5\text{GeTe}_2$ , *Appl. Phys. Lett.* **116**, 202402 (2020).
- [26] A. F. May, M.-H. Du, V. R. Cooper, and M. A. McGuire, Tuning magnetic order in the van der Waals metal  $\text{Fe}_5\text{GeTe}_2$  by cobalt substitution, *Phys. Rev. Mater.* **4**, 074008 (2020).
- [27] H. Zhang, D. Raftrey, Y. T. Chan, Y.-T. Shao, R. Chen, X. Chen, X. Huang, J. T. Reichanadter, K. Dong, S. Susarla, L. Caretta, Z. Chen, J. Yao, P. Fischer, J. B. Neaton, W. Wu, D. A. Muller, R. J. Birgeneau, and R. Ramesh, Room-temperature skyrmion lattice in a layered magnet  $(\text{Fe}_{0.5}\text{Co}_{0.5})_5\text{GeTe}_2$ , *Sci. Adv.* **8**, eabm7103 (2022).
- [28] T. Ohta, K. Kurokawa, N. Jiang, K. Yamagami, Y. Okada, and Y. Niimi, Enhancement of spin-flop-induced magnetic hysteresis in van der Waals magnet  $(\text{Fe}_{1-x}\text{Co}_x)_5\text{GeTe}_2$ , *Appl. Phys. Lett.* **122**, 152402 (2023).
- [29] D. Yuan, S. Jin, N. Liu, S. Shen, Z. Lin, K. Li, and X. Chen, Tuning magnetic properties in quasi-two-dimensional ferromagnetic  $\text{Fe}_{3-y}\text{Ge}_{1-x}\text{As}_x\text{Te}_2$  ( $0 \leq x \leq 0.85$ ), *Mater. Res. Express* **4**, 036103 (2017).
- [30] G. Zhang, F. Guo, H. Wu, X. Wen, L. Yang, W. Jin, W. Zhang, and H. Chang, Above-room-temperature strong intrinsic ferromagnetism in 2D van der Waals  $\text{Fe}_3\text{GaTe}_2$  with large perpendicular magnetic anisotropy, *Nat. Commun.* **13**, 5067 (2022).
- [31] See Supplemental Material at <http://link.aps.org/supplemental/10.1103/PhysRevB.109.104402> for more details about EDS, the derivative of the  $\chi$ - $T$  curves,  $M_R/M_S$ , the derivative of the  $\rho$ - $T$  curves, and carrier density  $n_e$  for  $(\text{Fe}_{1-x}\text{Co}_x)_3\text{GaTe}_2$  ( $0 \leq x \leq 0.55$ ) and  $(\text{Fe}_{1-x}\text{Ni}_x)_3\text{GaTe}_2$  ( $0 \leq x \leq 0.46$ ) single crystals.
- [32] K. Binder and A. P. Young, spin-glasses: Experimental facts, theoretical concepts, and open questions, *Rev. Mod. Phys.* **58**, 801 (1986).
- [33] Y. Luo, C. Cao, B. Si, Y. Li, J. Bao, H. Guo, X. Yang, C. Shen, C. Feng, and J. Dai,  $\text{Li}_2\text{RhO}_3$ : A spin-glassy relativistic Mott insulator, *Phys. Rev. B* **87**, 161121(R) (2013).
- [34] S. J. Li, D. Zhao, S. Wang, S. T. Cui, N. Z. Wang, J. Li, D. W. Song, B. L. Kang, L. X. Zheng, L. P. Nie, Z. M. Wu, Y. B. Zhou, M. Shan, Z. Sun, T. Wu, and X. H. Chen, Emergent spin-glass state in the doped Hund's metal  $\text{CsFe}_2\text{As}_2$ , *Phys. Rev. B* **107**, 115144 (2023).
- [35] B. Cheng, B. F. Hu, R. H. Yuan, T. Dong, A. F. Fang, Z. G. Chen, G. Xu, Y. G. Shi, P. Zheng, J. L. Luo, and N. L. Wang, Field-induced spin-flop transitions in single-crystalline  $\text{CaCo}_2\text{As}_2$ , *Phys. Rev. B* **85**, 144426 (2012).
- [36] X. Y. Tan, V. O. Garlea, K. Kovnir, C. M. Thompson, T. S. Xu, H. B. Cao, P. Chai, Z. P. Tener, S. S. Yan, P. Xiong, and M. Shatruk, Complex magnetic phase diagram with multistep spin-flop transitions in  $\text{La}_{0.25}\text{Pr}_{0.75}\text{Co}_2\text{P}_2$ , *Phys. Rev. B* **95**, 024428 (2017).
- [37] A. Tan, V. Labracherie, N. Kunchur, A. U. B. Wolter, J. Cornejo, J. Dufouleur, B. Büchner, A. Isaeva, and R. Giraud, Metamagnetism of weakly coupled antiferromagnetic topological insulators, *Phys. Rev. Lett.* **124**, 197201 (2020).
- [38] A. A. Isaeva, O. N. Makarevich, A. N. Kuznetsov, T. Doert, A. M. Abakumov, and G. Van Tendeloo, Mixed tellurides  $\text{Ni}_{3-x}\text{GaTe}_2$  ( $0 \leq x \leq 0.65$ ): Crystal and electronic structures, properties, and nickel deficiency effects on vacancy ordering, *Eur. J. Inorg. Chem.* **2010**, 1395 (2010).
- [39] H.-J. Deiseroth, K. Aleksandrov, C. Reiner, L. Kienle, and R. K. Kremer,  $\text{Fe}_3\text{GeTe}_2$  and  $\text{Ni}_3\text{GeTe}_2$  - two new layered transition-metal compounds: Crystal structures, HRTEM investigations, and magnetic and electrical properties, *Eur. J. Inorg. Chem.* **2006**, 1561 (2006).
- [40] A. N. Kuznetsova, E. A. Stroganovaa, E. Y. Zakharovaa, A. V. Solopchenkoa, A. V. Soboleva, I. A. Presniakova, D. I. Kirdyankinb, and V. M. Novotortsevb, Mixed nickel-gallium tellurides  $\text{Ni}_{3-x}\text{GaTe}_2$  as a matrix for incorporating magnetic cations: A  $\text{Ni}_{3-x}\text{Fe}_x\text{GaTe}_2$  series, *J. Solid State Chem.* **250**, 90 (2017).
- [41] N. Lenbrito, E. D. Bauer, F. Ronning, J. D. Thompson, and R. Movshovich, Magnetic microstructure and magnetic properties of uniaxial itinerant ferromagnet  $\text{Fe}_3\text{GeTe}_2$ , *J. Appl. Phys.* **120**, 1001 (2016).
- [42] H. B. Ahn, S. G. Jung, H. Lim, K. Kim, S. Kim, T. E. Park, T. Park, and C. Lee, Giant coercivity enhancement in a room-temperature van der Waals magnet through substitutional metal-doping, *Nanoscale* **15**, 11290 (2023).